Connectivity effects on fluid age and residence time distributions in two- and three-dimensional pore networks

Shahram Asgari

Department of Marine Sciences, University of Georgia, Athens, GA 30602, USA

Email: shahram.asgari@uga.edu

ORCID: 0009-0004-3810-2739

This is a non-peer-reviewed preprint submitted to EarthArXiv. It has not undergone peer review. The manuscript is intended for submission to the peer-reviewed journal Geoscientific Model Development.

Connectivity effects on fluid age and residence time distributions in two- and three-dimensional pore networks

Shahram Asgari

Department of Marine Sciences, University of Georgia, Athens, GA 30602, USA

Correspondence: shahram.asgari@uga.edu

Abstract

Pore-scale simulations are often run on a single plane cut from a three-dimensional image, because resolving the whole pore space is expensive. This study asks what that shortcut costs. What is at stake is the distribution of fluid ages, and above all its long tail, because that tail is what slow reactions respond to. We computed the distribution directly from the flow field, by labeling the fluid with its age and carrying one transport equation for every age. The first two moments of that equation give the mean age and the coefficient of variation (CV) of the age distribution. Solved numerically, they return the analytical mean age exactly and the analytical age variance to within 0.11 % for Pe ≥ 20. The same equations were then applied to two pore networks that are identical apart from the number of throats meeting at each pore, four in the flat network and six in the cubic one. With every throat open the two agree to 5 % in CV and 2.5 % in the upper tail, so dimension by itself changes little. Blocking throats at random changes this. At 45 % blocked, the flat network places the upper tail 3.8 times too high and leaves 5.4 times more pore volume without flow. Spanning probabilities measured on the same grids explain the difference. The flat grid loses its connected paths between 50 and 60 % blocked, while the cubic grid still spans at 70 %. In the blocked networks the resolved tail is a power law, with an exponent of -2.4 for the flat grid against -5.9 for the cubic one. What controls the old-water tail is therefore how well the pore space is connected, not how many dimensions are resolved. A flat section may be used where the pore space is comfortably connected, and should not be where it is not.

Article Highlights

- Carrying a separate transport equation for each fluid age delivers the mean age and the age variance straight from the flow field, and both match their known solutions to within 0.11 % for Pe ≥ 20.
- With every throat open a flat pore network matches a cubic one, but with 45 % of throats blocked it places the old-water tail 3.8 times too high.
- Spanning probabilities measured on the same grids trace that error to lost connections, the flat grid failing between 50 and 60 % of throats blocked while the cubic grid survives to 70 %.

Keywords Residence time distribution, Fluid age, Pore-scale modeling, Pore network, Connectivity, Percolation, Péclet number

1. Introduction

Whether a solute dissolves a mineral, attaches to a grain surface or is taken up by microbes depends on how long it stays in contact with that surface. Simulations that resolve the flow in individual pores are now the usual way to predict this contact time (Blunt et al. 2013; Bijeljic et al. 2013). They deliver it in two forms, the arrival times of a tracer at the outlet and the ages of the fluid held inside the domain (Dentz et al. 2011). Neither form is recovered from a mean velocity or a mean travel time (Ginn 1999). What makes such simulations worth their cost is that the wide range of velocities among pores produces early arrival, long tailing and other non-Fickian behavior that a Darcy-scale description smooths away (Bijeljic et al. 2011; Berkowitz et al. 2006). Two mechanisms produce that spread. Even within a single tube, dispersion rises steeply with velocity, as the classical result of Taylor (1953) and Aris (1956) shows (Bear 1972). Across a pore network the stronger effect is the range of velocities among pores, with fast channels delivering the early arrivals and slow or dead-end pores delivering the old tail, which is the behavior that continuous-time random-walk models were built to describe (Metzler and Klafter 2000; Le Borgne et al. 2008).

Resolving the pore space in all three dimensions is expensive, and one common economy is to work on a single plane cut from a micro-CT image. A plane, however, cannot carry the connections that leave it. Where a grain blocks the way, fluid in a full sample can pass above or below it, whereas fluid confined to a plane has no such route (Renard and Allard 2013). What this costs has been measured for permeability and for the mean arrival time. It has not been measured for the long tail of the age distribution, which is fed by the slowest and least connected pores and which is precisely what slow reactions respond to (Ginn 1999; Le Borgne et al. 2008). Whether a plane may be substituted for the full pore space is therefore still settled by argument rather than by measurement.

The theory required for that measurement is already available. Danckwerts (1953) put the distribution of residence times on a firm footing for chemical reactors. The geosciences arrived at the same footing through the age and residence time theory built for ocean and groundwater models, which carries a transport equation for fluid labeled by its age (Delhez et al. 1999; Deleersnijder et al. 2001; Cornaton and Perrochet 2006). One such equation, solved on the flow grid, returns the mean age (Goode 1996; Varni and Carrera 1998). The same framework supports environmental-tracer ages (Cornaton and Perrochet 2006) and transit time distributions in catchment hydrology (Botter et al. 2011; Rinaldo et al. 2015; Harman 2015). We say at the outset that these age-moment and transform relations are established results, and that the analytical limits used below belong to Danckwerts (1953) and to Kreft and Zuber (1978), so deriving them is not our contribution. Two things have not been tested. The first is whether those equations, solved on a flow field rather than on paper, return their own analytical limits. The second is how much of the age distribution is lost when the pore space is reduced to a plane.

The present study answers both. We compute the whole distribution of fluid ages from the flow field itself and then test how faithfully a plane reproduces it. The method is to label the fluid by its age. Instead of tracking the total amount of solute, we sort each parcel by how long it has been inside the domain and write one transport equation for each age. Aging then enters that equation as a steady drift along the age axis, because fluid that is not replaced grows older at the rate of the clock. Taking the first two moments of that equation gives the mean age and the CV of the age distribution, and a transform in the age variable carries the whole distribution instead of a few summary numbers. We solve these equations first in a 1D column, where the answers are known, and then on pore networks assembled from pores joined by throats of randomly assigned conductance. One network is flat, with four throats meeting at each pore, and the other is cubic, with six. Blocking throats at random removes connections, as cementation does in natural rock. A separate particle-tracking experiment then splits apart two effects the networks combine, the spread of the pore velocities and the distance a particle travels before its velocity changes. On this basis we address three questions. These are (i) whether the moment equations return the analytical CV, and whether that agreement depends on the outlet condition, (ii) how far a flat section misstates the oldest water leaving the sample as connections are removed, and what property of the pore space controls that error, and (iii) how velocity spread and velocity correlation length act separately on the CV.

2. Methods

2.1. Age-Resolved Transport Equations

The whole distribution of ages is resolved by labeling the fluid and following each age separately. We write $C(x, \tau, t)$ for the age-resolved concentration, meaning the amount of solute carried per unit volume of fluid whose age lies between τ and $\tau + d\tau$. The age τ is simply the time that has passed since that fluid entered the domain. Summing over all ages returns the ordinary concentration, which is therefore the zeroth age moment,

$$c(x, t) = \int_0^\infty C(x, \tau, t)\, d\tau \,, \tag{1}$$

where c is the ordinary solute concentration that a standard transport model carries, C is the age-resolved concentration, x is position, t is time and τ is the age. The first moment of C defines the age concentration α and the mean age a,

$$\alpha(x, t) = \int_0^\infty \tau\, C(x, \tau, t)\, d\tau \,, \quad a(x, t) = \alpha / c \,. \tag{2}$$

where α is the age concentration, meaning the solute weighted by how old it is, and a is the mean age of the fluid at that point, obtained by dividing α by c.

The fluid moves through the pore space with velocity u (with $\nabla \cdot u = 0$) and the solute disperses with coefficient D. Fluid of a given age is advected and dispersed exactly like an ordinary solute. Only one thing is added. Every parcel grows older at the rate of the clock, so age is itself transported toward older values at unit speed. That adds the term $\partial C/\partial \tau$ and gives the aging equation (Delhez et al. 1999; Deleersnijder et al. 2001),

$$\partial C/\partial t + \partial C/\partial \tau + \nabla \cdot (u\, C) - \nabla \cdot (D\, \nabla C) = 0 \,. \tag{3}$$

where u is the pore velocity, D is the dispersion coefficient, $\nabla \cdot$ is the divergence operator, and $\partial C/\partial \tau$ is the transport of fluid along the age axis. That last term is the only difference from an ordinary advection–dispersion equation.

Three conditions close the problem. Fluid enters with zero age, which sets $C(\tau) = c\, \delta(\tau)$ at the inlet. Nothing is infinitely old, so $C \to 0$ as $\tau \to \infty$. And no new fluid appears inside the domain, so $C(x, 0, t) = 0$ everywhere in the interior. Integrating Eq. (3) over all ages then removes the $\partial C/\partial \tau$ term and returns the ordinary transport equation for c,

$$\partial c/\partial t + \nabla \cdot (u\, c) - \nabla \cdot (D\, \nabla c) = 0 \,, \tag{4}$$

where c is again the ordinary concentration of Eq. (1), so that Eq. (4) is nothing more than the standard advection–dispersion equation. This confirms that the labeling adds no new physics to the transport itself. Every derivation in this section is set out step by step in Appendix A.

Weighting Eq. (3) by τ and integrating over all ages produces a transport equation for the age concentration, driven by a uniform source. This is the direct age equation of Goode (1996),

$$\partial\alpha/\partial t + \nabla\cdot(u\ \alpha) - \nabla\cdot(D\ \nabla\alpha) = c\ , \tag{5}$$

where α is the age concentration of Eq. (2) and the source c on the right-hand side is the ordinary concentration, which appears because every parcel ages at unit rate. Dividing its solution by c gives the mean age everywhere on the flow grid (Goode 1996; Varni and Carrera 1998). The mirror image of the age is the life expectancy, which is the time a parcel still has to spend before it leaves. It comes from the same problem solved backward, with the flow reversed and the inlet and outlet exchanged (Cornaton and Perrochet 2006). Writing e for the mean life expectancy,

$$-\nabla\cdot(u\ e) - \nabla\cdot(D\ \nabla e) = 1\ . \tag{6}$$

where e is the mean life expectancy and the unit source on the right-hand side is the rate at which life expectancy is used up, one second per second.

A parcel passing a given point has a residence time equal to its age plus its life expectancy, so the residence time distribution combines the two fields. Weighting Eq. (3) by τ^n instead, and writing $\mu_n = \int_0^\infty \tau^n\ C\ d\tau$ for the n-th age moment, gives a recursion at steady state in which every moment is driven by the one below it,

$$\nabla\cdot(u\ \mu_n) - \nabla\cdot(D\ \nabla\mu_n) = n\ \mu_{n-1}\ . \tag{7}$$

where μ_n is the n-th age moment, μ_{n-1} is the moment one order below it and n is the order of the moment. The zeroth moment has no source. The first is driven by c and returns the mean age. The second is driven by 2 α and returns the age variance,

$$\sigma_a^2 = \mu_2 / c - a^2\ . \tag{8}$$

where σ_a^2 is the variance of the age distribution, μ_2 is the second age moment from Eq. (7), c is the concentration from Eq. (1) and a is the mean age from Eq. (2).

Equation (8) makes clear that dispersion is what creates the spread of ages. Set D to zero and the recursion carries a single age along each streamline, leaving σ_a^2 at zero. It is diffusion and mechanical dispersion, mixing parcels that took different paths, that broaden the distribution (Kitanidis 1994). We report this spread throughout as the coefficient of variation (CV), the standard deviation divided by the mean, which measures width without reference to timescale.

The moments compress the distribution into a few numbers. Its whole shape is carried instead by a Laplace transform in the age variable, $\hat{C}(x, s) = \int_0^\infty C\ e^{-s\tau}\ d\tau$, which turns the aging term into a multiplication and gives, at steady state,

$$s\ \hat{C} + \nabla\cdot(u\ \hat{C}) - \nabla\cdot(D\ \nabla\hat{C}) = 0\ . \tag{9}$$

where $\hat{C}$ is the Laplace transform of C in the age variable and s is the transform variable, which has units of inverse time. Here s behaves exactly as a decay rate applied uniformly, so the transformed problem is the response of the medium to a tracer decaying everywhere at rate s.

Read at the outlet, $\hat{C}$ carries the entire residence time distribution, and its derivatives at the origin return the moments,

$$\langle \tau^n \rangle = (-1)^n \, d^n \hat{C} / d s^n \,|_{s=0} \,. \tag{10}$$

where $\langle \tau^n \rangle$ is the n-th moment of the residence time distribution and the derivative is evaluated at s = 0. Small values of s fix the mean and the CV. The slowest-decaying part of $\hat{C}$ fixes the long old-water tail. Should the domain drain through one slowest mode that stands well apart from the rest, that tail decays as $\exp(-\lambda_1 \tau)$, with λ_1 set by the most poorly flushed regions. Such a separation is not guaranteed, so we treat the exponential form as conditional and measure λ_1 in Sect. 3.4 rather than assume it.

One distinction has to be drawn before any of these fields is compared with a breakthrough curve, because an age can be averaged in two ways that do not agree. The moments of Eqs. (2), (5) and (7) average over the fluid sitting in a volume, giving the resident average. A breakthrough curve averages over the fluid crossing a surface and weights each pore by the flow it carries, giving the flow-weighted average. Kreft and Zuber (1978) showed that the two produce different distributions for one and the same transport problem. Section 3.3 measures how far apart they lie on our networks.

2.2. Analytical Limits

To fix the behavior that the numerical solutions have to reproduce, we evaluated the equations of Sect. 2.1 in three idealized geometries. These bracket everything that can happen in between. With advection only (D = 0) along a path of length L at speed v, every parcel shares one history and the residence time distribution collapses to a single spike,

$$g(\tau) = \delta(\tau - L/v) \,, \quad CV = 0 \,. \tag{11}$$

where $g(\tau)$ is the residence time distribution, δ is the Dirac delta function, which places all the fluid at a single time, L is the path length, v is the flow speed and CV is the coefficient of variation.

At the other extreme, mixing fast enough to hold the interior uniform makes the outflow a fair sample of everything inside, and the distribution becomes exponential (Danckwerts 1953),

$$g(\tau) = (1/T)\, e^{-\tau/T} \,, \quad CV = 1 \,, \tag{12}$$

where T is the mean residence time, equal to the fluid volume divided by the volumetric flow rate. Between the two, 1D transport at constant velocity v with dispersion D over a distance L gives the inverse-Gaussian distribution, which is the first-passage density of a drifting diffusion (Kreft and Zuber 1978),

$$g(\tau) = \sqrt{L^2 / (4 \pi D \tau^3)} \, \exp(-(L - v\tau)^2 / (4 D \tau)) \,, \tag{13}$$

where τ is the residence time, D is the dispersion coefficient and L and v are the path length and flow speed of Eq. (11). This distribution has mean L/v and variance $2 D L / v^3$. Its squared coefficient of variation collapses to one number,

$$CV^2 = 2 D / (v L) = 2 / Pe \,, \tag{14}$$

where CV is the coefficient of variation of the residence time and Pe = v L / D is the Péclet number, which compares advective with dispersive transport. Equation (14) is the leading term of the variance that the method of moments extracts from the axial-dispersion model (van der Laan 1958; Levenspiel 1999), a link we return to in Sect. 3.1. The three limits behave as Eq. (14) requires. The distribution sharpens from a broad, early-arriving and heavy-tailed shape at low Pe toward the plug-flow spike at high Pe (Fig. 1). Its CV stays between the well-mixed and plug-flow bounds across the whole range examined (Fig. 2a), and the breakthrough curves steepen to match (Fig. 2b).

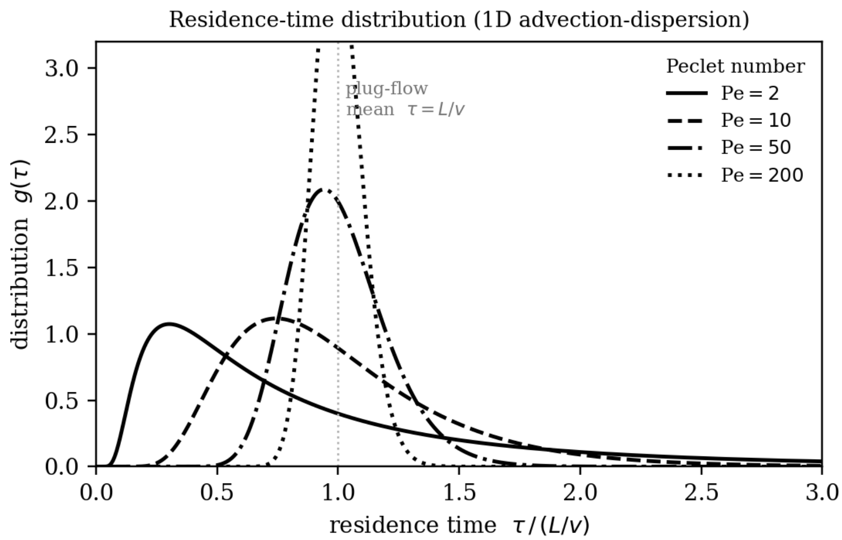

Figure 1. Residence time distribution for 1D advection–dispersion, given by the inverse-Gaussian first-passage density of Eq. (13) and plotted against residence time normalized by the advective mean L/v, for Péclet numbers 2, 5, 20 and 100. As Pe increases the distribution narrows toward the plug-flow limit, and as Pe decreases it broadens and skews toward early arrival with a long tail, approaching the well-mixed limit. The CV of each curve follows Eq. (14)

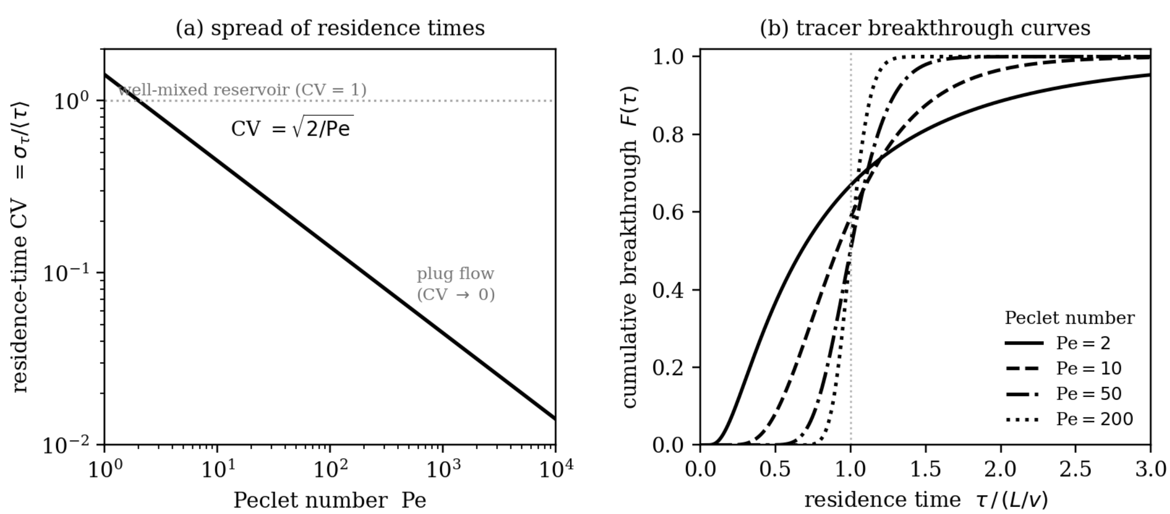

Figure 2. Péclet control of the residence time distribution from the analytical limits of Sect. 2.2. (a) Coefficient of variation of the residence time on logarithmic axes, bounded by the well-mixed limit (CV = 1) and the plug-flow limit (CV = 0). (b) Cumulative breakthrough curves, where a low Péclet number produces early arrival and long tailing and a high Péclet number a sharp front at the advective mean

One qualification attaches to these limits, and it is the open-vessel and closed-vessel question raised by Danckwerts (1953) and by Kreft and Zuber (1978). Solving Eq. (5) in 1D with a zero-age inlet gives a mean age a(x) = x/v that does not depend on the dispersion coefficient. That holds only where the fluid is free to leave with the flow, as it is in a semi-infinite column. Close the outlet to diffusion and the outlet mean age becomes

$$a(L) = L/v - (D/v^2)(1 - e^{-Pe}) , \tag{15}$$

where a(L) is the mean age at the outlet, L/v is the value it would take with an open outlet and the second term is the deficit introduced by closing it, a deficit of order 1/Pe. We therefore imposed both outlet conditions in the numerical solutions of Sect. 3.1, and we quote a = x/v below together with the outlet condition it assumes.

2.3. Pore-Network Model

The pore networks place pores on a regular grid and join nearest neighbors with throats. The flat network is a square grid with four throats meeting at each pore, and the cubic network has six. Every throat carries a conductance, which measures how easily it passes fluid, drawn from the same log-normal distribution in both networks (σ = 1 about a unit median). The two networks share the flow-direction length of 60 pores, the blocking fraction, and the pore count to within 2 % (48 000 against 47 040, since the cubic grid must have a whole number of pores across its section). They cannot share cross-sectional shape, aspect ratio or total throat count, which is unavoidable once the number of throats per pore changes. The comparison is therefore controlled on flow length, throat conductance and pore count, and not on every geometric measure.

A unit pressure difference drives flow between the inlet and outlet faces, the lateral faces pass no flow, and mass conservation fixes the pressure at every pore. Pores that form a group with no path from inlet to outlet carry no through-flow and were excluded. The flow in each throat then follows from the pressure drop across it. To degrade connectivity we blocked a fraction p_b of the throats at random, which produces dead ends and isolated pockets in the way that cementation or fine-scale plugging does.

How much damage a given blocking fraction does depends on the grid. A connected path survives only while enough throats remain open, and that threshold is about 0.5 on a square lattice against about 0.2488 on a simple cubic one (Stauffer and Aharony 1994). The same blocking fraction therefore leaves the two networks at very different distances from failure. We measured that distance instead of assuming it, computing the spanning probability and the connected pore fraction over ten realizations at each blocking fraction, and repeating the exercise at half the domain size as a finite-size check.

On each network we solved the network form of Eq. (5) for the mean age and of Eq. (7) for the second age moment. Both were obtained by a single sweep through the pores in order of decreasing pressure, which is exact here because potential flow runs downhill in pressure and the flow graph is therefore acyclic. Every configuration was repeated with five realizations of the random throats, so that the scatter between them can be reported.

2.4. Particle Tracking and Velocity Correlation

The full residence time distribution was obtained independently of the moment equations. We released 40 000 particles at the inlet and recorded when each reached the outlet. Every pore was treated as well mixed, so the time a particle spends inside it is drawn from an exponential distribution whose mean is the pore volume divided by the through-flow, which applies the Eq. (12) limit at pore level. A dead-end pore carries no net flux in steady flow of an incompressible fluid, so no particle is ever routed into one. Such pores are counted in the stagnant pore fraction, and the tracked distribution is the distribution of the mobile fluid. We also report how many particles never reach the outlet, so that censoring cannot go unnoticed.

A pore network mixes two effects that a simpler setting can hold apart, the spread of the pore velocities and the distance a particle travels before its velocity changes. To separate them we tracked particles through a 1D domain in which each particle carries a log-normal velocity with $\sigma_v = 0.6$ and redraws it every correlation length ℓ_c. Letting ℓ_c grow without bound produces a bundle of stream tubes that never exchange fluid. A finite ℓ_c instead lets a particle forget its velocity, as it does in a real pore network. Running the same routine with all velocities equal advances the advection–dispersion process by the Euler–Maruyama scheme and supplies the check of the integrator reported in Sect. 3.1.

2.5. Numerical Controls

The controls used to obtain the results are reported here so that they can be reproduced. The 1D moment solves use 4001 nodes on a unit domain with $v = 1$ and D between 0.01 and 0.2. The particle tracking uses 20 000 particles for the correlation-length sweep and 40 000 for the networks, with seeds 7 to 11, a cut-off of 40 mean transit times and a log-normal velocity spread $\sigma_v = 0.6$. The time step is scaled with the dispersion coefficient, so that the diffusive step is always the same small fraction of the domain. The pore networks use 60 pores along the flow direction, 48 000 pores in total, log-normal throat conductances with $\sigma = 1$, blocked fractions of 0 to 45 %, and five realizations each.

Convergence was checked at $Pe = 100$ in both the number of particles and the time step. The CV moves from 0.1393 at 5000 particles to 0.1415 at 20 000 and 0.1406 at 80 000. It moves from 0.1419 at a time step of 1.6×10^{-3} to 0.1415 at 8×10^{-4} and 0.1425 at 4×10^{-4}. Every one of these values sits within about 1 % of the analytical form and inside the sampling noise. All computations were carried out in Python with NumPy and SciPy.

3. Results and Discussion

3.1. Verification of the Moment Equations

The equations were checked against the analytical limits of Sect. 2.2 before being taken to pore structure. The analytical CV can first be set against the residence time results of classical reactor engineering, which the method of moments extracts from the axial-dispersion model. For a vessel of finite length the exact variance depends on how the inlet and outlet are treated. An open vessel gives 2/Pe + 8/Pe^2 (van der Laan 1958; Levenspiel 1999) and a closed one gives 2/Pe − (2/Pe^2)(1 − e^{-Pe}) (Danckwerts 1953). At Pe = 100 these depart from Eq. (14) by 4 % and 1 % respectively, and both converge to it for Pe ≳ 10 (Fig. 3a). Figure 3b shows the three bracketing distributions of Sect. 2.2 together.

This comparison proves less than it appears to, and we say so plainly. Equation (14) is the leading term of both of those expressions, and Eq. (13) solves the very axial-dispersion equation whose moments van der Laan computed. Their agreement is forced by the algebra and is not independent evidence. What it does establish is which outlet condition Eq. (14) belongs to, namely the open vessel at high Péclet number.

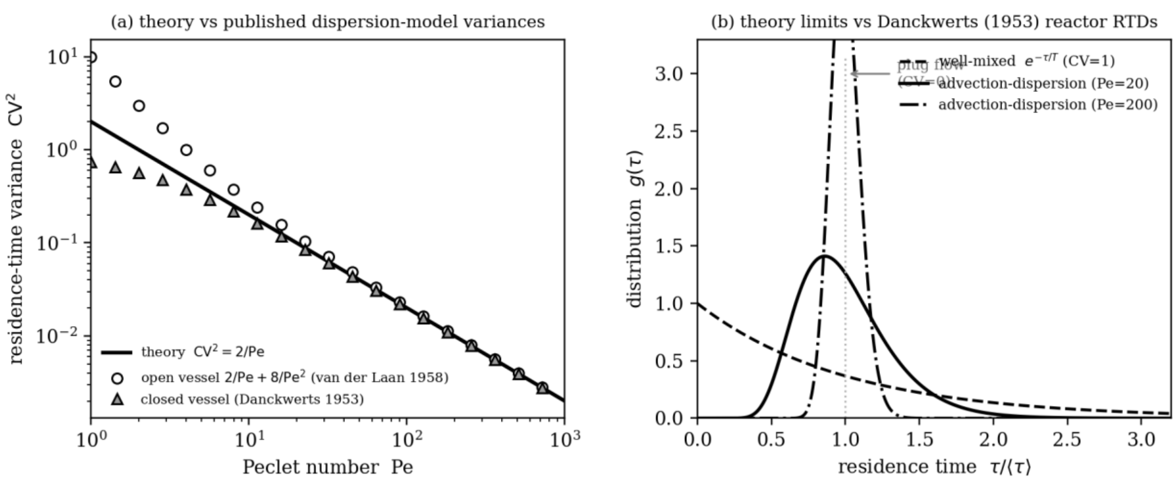

Figure 3. Consistency with classical dispersion-model and reactor residence time results. (a) The analytical form CV^2 = 2/Pe (line) against the exact dispersion-model variances of the open vessel (van der Laan 1958; Levenspiel 1999) and the closed vessel (Danckwerts 1953), all of which converge for Pe ≳ 10 because 2/Pe is the leading term of both. (b) The three bracketing distributions of Sect. 2.2, namely the perfectly mixed exponential (CV = 1), the inverse-Gaussian at Pe = 20 and 200, and the plug-flow spike (CV = 0), reproducing the canonical reactor distributions of Danckwerts (1953)

The test that does probe the formulation of Sect. 2.1 is to solve its own equations numerically. We solved Eq. (5) for the mean age and Eq. (7) with n = 2 for the second moment, in 1D steady advection–dispersion with a zero-age inlet and fluid free to leave with the flow. Away from the boundary layer at the outlet, the numerical mean age returns x/v to within 0.000 % at every Péclet number tested. The variance from Eq. (8) returns 2 D x / v^3 to 0.11 % at Pe = 20 and to better than 0.005 % at Pe = 50 and above (Table 1, Fig. 4a). CV^2 = 2/Pe therefore follows from the moment equations by themselves, with no appeal to the analytical density of Eq. (13). That answers the first of the three questions posed in Sect. 1.

Table 1. Numerical verification of Eqs. (5), (7) and (8) against the analytical limits, and of the closed-outlet correction of Eq. (15). Errors are evaluated at x = 0.8 L, away from the boundary layer at the outlet. The variance error remaining at Pe = 5 originates in that layer, which occupies a larger share of the domain at low Péclet number

Pe	**mean-age error**	**variance error**	**closed-outlet a(L)**	**Eq. (15)**	**deficit**	**CV^2 from Eqs. (5),**	**2/Pe**

						(7), (8)	
5	0.000 %	9.03 %	0.8012	0.8013	19.9 %	0.400000	0.400000
10	0.000 %	1.69 %	0.8999	0.9000	10.0 %	0.200000	0.200000
20	0.000 %	0.11 %	0.9499	0.9500	5.0 %	0.100000	0.100000
50	0.000 %	0.00 %	0.9799	0.9800	2.0 %	0.040000	0.040000
100	0.000 %	0.00 %	0.9899	0.9900	1.0 %	0.020000	0.020000

The second half of that question concerns the outlet, and here the answer is that it matters at low Péclet number. Solving the same equations with a closed outlet returns Eq. (15) to three decimal places. The resulting deficit in the outlet mean age reaches 19.9 % at Pe = 5 and falls to 1.0 % at Pe = 100 (Table 1). Quoting a = x/v without qualification is therefore safe only for an open outlet or at high Péclet number.

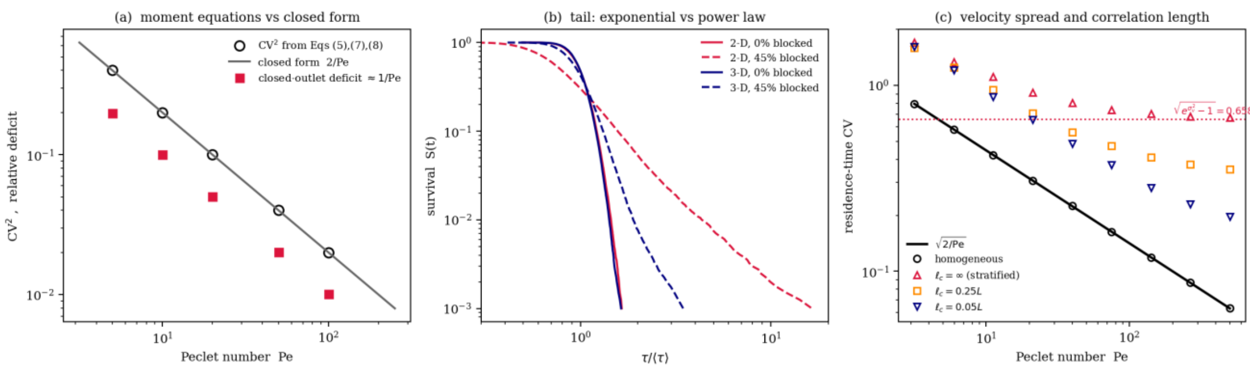

Figure 4. Verification of the moment equations and the two controls on the CV. (a) Squared coefficient of variation obtained by solving Eqs. (5), (7) and (8) numerically (circles) against the analytical form 2/Pe (line), with the closed-outlet deficit of Eq. (15) following 1/Pe (squares). (b) Survival curves of the simulated residence time distributions, where the resolved tail of a blocked network follows a power law and the 2D tail is the heaviest (Sect. 3.4). (c) Coefficient of variation of the residence time against Péclet number with all velocities equal and with log-normal velocity spread at three correlation lengths, the dotted line giving the analytical value for a bundle of unmixed stream tubes (Sect. 3.5)

The particle tracking used in Sects. 3.3 to 3.5 was checked separately. We tracked particles through the same 1D domain and recorded when each first reached the outlet. The simulated distributions reproduce the inverse-Gaussian density across Péclet numbers (Fig. 5a), and the simulated CV follows Eq. (14) to a mean relative error of 0.17 % and a maximum of 0.29 % over five seeds (Fig. 5b). These same runs supply the baseline for Sect. 3.5. As with the comparison above, the scope of this check is narrow. The inverse-Gaussian is by construction the exact first-passage law of the process the integrator advances, so what is verified is the integrator and the sampling, not the age formulation of Eqs. (3) to (10). That formulation is tested by the moment solves. An agreement quoted below one percent also needs a stated noise floor, and with 8000 particles the sampling standard error on a CV is of order 0.5 %, which is why we give the mean and the maximum over five seeds rather than a single number.

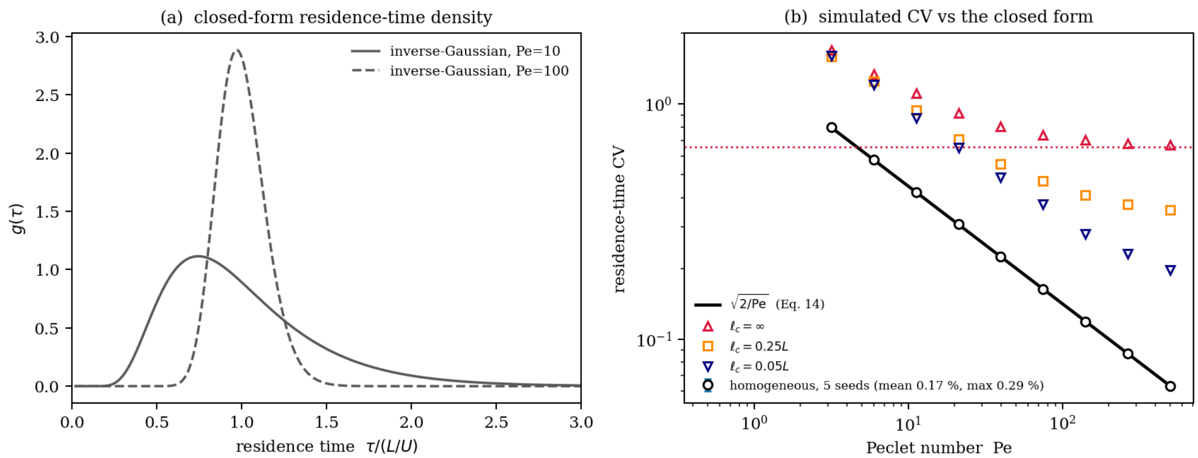

Figure 5. Verification of the particle tracking by comparison with the analytical first-passage law. (a) Simulated residence time distributions (histograms) for Péclet numbers 10 and 100 against the inverse-Gaussian densities (gray). (b) Coefficient of variation of the residence time against Péclet number, where the simulation with all velocities equal follows Eq. (14) to a mean of 0.17 % and a maximum of 0.29 % over five seeds, while log-normal velocity spread raises it above that form by an amount set by the correlation length (Sect. 3.5)

3.2. Connectivity of the 2D and 3D Networks

With the equations verified, we measured how far each network sits from losing its connected paths. That distance is what everything below depends on. The flat grid keeps a path across the sample in every realization up to 50 % of throats blocked. Past that point it fails quickly, the spanning probability dropping to 0.30 at 55 % and to zero at 60 %. Its connected pore fraction collapses in step, from 0.94 at 40 % blocked to 0.45 at 50 % and 0.006 at 55 %. The cubic grid behaves quite differently. It spans in every realization at every blocking fraction tested up to 70 %, and even there it still holds 0.65 of its pores in the connected cluster.

These measurements match the thresholds quoted in Sect. 2.3. The flat grid loses connection between 50 and 60 % blocked, which leaves 0.40 to 0.50 of its throats open and agrees with the square-lattice value of 0.5. The cubic grid still spans with only 0.30 of its throats open, in agreement with the cubic-lattice value of 0.2488 (Stauffer and Aharony 1994). Halving the domain moves the flat transition by less than one blocking increment, so it is not an artifact of system size. At any given blocking fraction the two networks therefore sit at very different distances from failure, and that is the mechanism the following sections examine.

3.3. Residence Time Distributions in 2D and 3D

Solving Eq. (7) on these networks exposes one limit on what the moment equations can deliver, which we quantify before the comparison itself. At full connectivity the flow-weighted outlet CV from Eqs. (5) and (7) tracks the particle-tracked value closely, 0.1648 against 0.1651 in 2D and 0.1575 against 0.1573 in 3D, an agreement within 0.2 %. Once throats are blocked the two part company by orders of magnitude, and the moment result climbs to 10^3 and beyond.

This is not a numerical failure. Blocking leaves pores that are still connected but almost still, with pore residence times $\theta = V/Q$ reaching 10^{10} to 10^{12} mean transit times. The resident age distribution genuinely holds fluid of that age. A finite particle ensemble, by contrast, never happens to enter a pore carrying so little flow. Equation (7) therefore returns the resident second moment including that nearly stagnant fluid, while particle tracking returns the distribution of the fluid that actually breaks through. Every statistic in Table 2 accordingly comes from particle tracking, and on the networks the moment equations are used only for the mean-age field of Fig. 6b.

The same split shows up in the outlet mean age, which settles the resident and flow-weighted question raised in Sect. 2.1. In a fully connected network the flow-weighted mean outlet age sits 2 to 3 % below the resident average, 2559 against 2627 in 2D and 2244 against 2309 in 3D, so the distinction does not matter. Block 35 % of the throats and it does. The flow-weighted value then sits 50 % above the resident average in 2D, 9805 against 6536, and 44 % above it in 3D, 5358 against 3733. The few surviving high-flow channels are carrying fluid older than the average outlet pore. In every case the flow-weighted value is the one that matches the particle-tracked breakthrough, to within 2 to 9 %, so it is the quantity to use wherever a breakthrough curve is intended.

With those two points settled, the comparison is straightforward. At full connectivity the number of dimensions makes almost no difference (Table 2, first row), and the two flow fields are similarly well connected (Fig. 6a1). The CV is 0.165 in 2D against 0.157 in 3D, a difference of 5 %, and the upper-tail quantile is 1.64 ± 0.01 against 1.60 ± 0.02, a difference of 2.5 %. The tail quantiles therefore overlap within about two realization standard deviations. This case is the control, because any larger difference appearing at lower connectivity has to be attributed to connectivity rather than to dimension. As throats are blocked the two networks pull apart steadily (Table 2, Fig. 6d). At 45 % blocked the flat upper-tail quantile is 12.39 against 3.27 in 3D, a factor of 3.8, and the stagnant pore fraction is 14.5 % against 2.7 %, a factor of 5.4.

Table 2. Residence time statistics on matched 2D and 3D pore networks as throats are blocked. CV is the coefficient of variation and τ_{99} and $\tau_{99.9}$ are the upper-tail quantiles, all normalized by the mean residence time, while the stagnant column gives the fraction of pores carrying no flow. Uncertainties are standard deviations over five realizations. The two networks share flow length, pore count and throat conductance to within 2 %, and differ in the number of throats per pore, four against six, and unavoidably in cross-section and total throat count. No particles failed to reach the outlet in any case. The 45 % 2D row sits close to the point at which connected paths are lost, where the variation from one realization to the next is large, so its uncertainties should be read as evidence of that closeness rather than as a precise estimate

Blocked	**2D CV**	**2D τ_{99}**	**2D $\tau_{99.9}$**	**2D stagnant**	**3D CV**	**3D τ_{99}**	**3D $\tau_{99.9}$**	**3D stagnant**
0 %	0.165 ± 0.001	1.44 ± 0.01	1.64 ± 0.01	0.0 %	0.157 ± 0.001	1.42 ± 0.00	1.60 ± 0.02	0.0 %
15 %	0.233 ± 0.008	1.66 ± 0.01	2.45 ± 0.06	0.6 %	0.186 ± 0.007	1.51 ± 0.01	1.86 ± 0.05	0.5 %
25 %	0.328 ± 0.022	1.93 ± 0.01	3.58 ± 0.20	1.4 %	0.214 ± 0.005	1.61 ± 0.01	2.23 ± 0.06	0.9 %
35 %	0.481 ± 0.036	2.39 ± 0.02	5.09 ± 0.12	3.9 %	0.277 ± 0.023	1.73 ± 0.01	2.74 ± 0.15	1.4 %
45 %	3.69 ±	3.87 ±	12.39 ±	14.5 %	0.367 ±	1.88 ±	3.27 ±	2.7 %

4.90	0.27	2.38		0.121	0.01	0.17

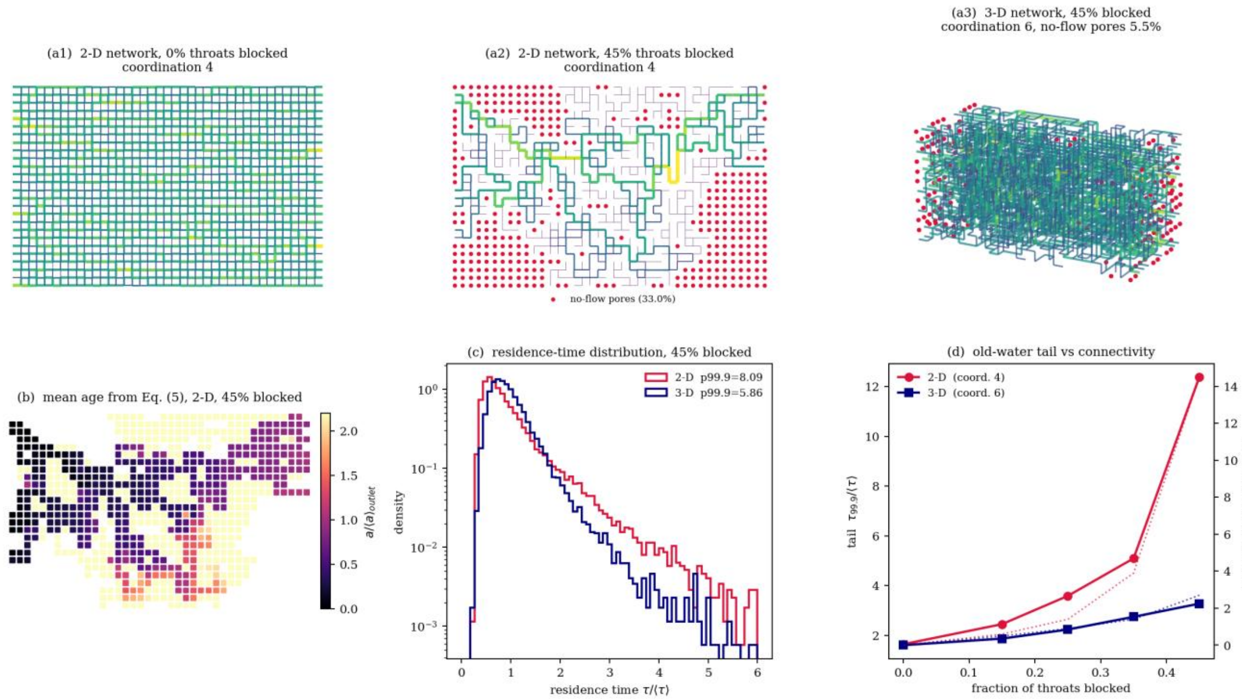

Figure 6. Pore networks and the effect of connectivity. (a1) 2D network with all throats open, where throat color and thickness show the flow magnitude. (a2) The same network with 45 % of throats blocked, where the flow has collapsed onto a few tortuous channels and a third of the pores (red) are stagnant. (a3) 3D network at the same 45 % blocking, still densely connected and with far fewer stagnant pores. (b) Mean age from Eq. (5) on the blocked 2D network, normalized by the outlet mean, where pale regions are old water in poorly flushed pockets. (c) Residence time distributions on logarithmic axes, where the 2D tail is visibly heavier. (d) Upper-tail quantile against blocked fraction, with the stagnant pore fraction shown dotted on the right axis

Two things about this divergence need explaining. The first is that it follows directly from the connectivity measured in Sect. 3.2. At 45 % of throats blocked the flat network is left with 55 % of its throats, barely above the 0.5 it needs to stay connected, whereas the cubic network sits far above its 0.249 and still offers many alternative routes (Fig. 6a2, a3). The second is the size of the flat uncertainty on the CV at that blocking, 3.69 ± 4.90, where the scatter between realizations exceeds the mean itself and shows up as the widest error bar in Fig. 6d. Since the network still spans the sample in every realization here (Sect. 3.2), the variability is not about whether a path exists. It comes from the surviving paths being few and their conductances widely spread, so the tail depends on which bottleneck happens to survive. A flat section close to the threshold does not merely misstate the tail, then. It gives an unpredictable one.

The direction of this result is the opposite of what one might expect. The expectation is that a 3D medium holds old water which a flat model would flush away. The computation shows the reverse. A flat section cannot route around blocked throats, so it forces the flow through a few tortuous paths and overstates both the old-water tail and the stagnant pore fraction. That answers the second of the three questions posed in Sect. 1.

3.4. Form of the Residence Time Tail

Section 2.1 predicts an exponential tail wherever one slowest mode stands well apart, while the non-Fickian literature reports power-law tails, so we tested which form the computed distributions support. For each realization we took the fraction of fluid still inside the sample at each time, which is the survival curve, and fitted both forms to its long right-hand end. The fitting window runs from the time exceeded by the slowest tenth of the fluid down to a surviving fraction of 10^{-3}. Each fit is reported with the range it spans and with the difference in coefficient of determination between the two forms, which acts as the discrimination statistic (Table 3).

Table 3. Tail fits to the network residence time distributions. Uncertainties are standard deviations over five realizations. At full connectivity the resolved tail reaches only about an eighth of a decade in τ and the two candidate forms differ by less than 0.005 in R^2. They cannot be told apart there, so we make no claim about the form of the tail in that case

Network	Blocked	Exponential λ_1	R^2 exp	Power-law exponent	R^2 power	Decades in τ	Favored
2D	0 %	10.56 ± 0.15	0.9986	−14.32 ± 0.18	0.9945	0.13	not resolved
3D	0 %	11.24 ± 0.11	0.9972	−15.01 ± 0.13	0.9924	0.12	not resolved
2D	45 %	0.65 ± 0.10	0.8766	−2.42 ± 0.18	0.9958	0.90	power law
3D	45 %	3.21 ± 0.24	0.9451	−5.89 ± 0.27	0.9885	0.40	power law

The answer differs sharply between the two connectivity regimes. At full connectivity the resolved tail is simply too short to decide. It spans about 0.12 decades in τ, the two fits differ by less than 0.005 in R^2, and the ordering is not even the same in the two networks. We therefore claim no exponential regime, and the conditional form of Sect. 2.1 stands untested. Once the pore space is blocked the decision is clear. Over 0.90 decades in 2D the power law beats the exponential by 0.12 in R^2, and the fitted exponent is −2.42 ± 0.18 in 2D against −5.89 ± 0.27 in 3D (Fig. 4b). The same contrast is visible directly in the two distributions (Fig. 6c). A shallower exponent means a heavier tail, so this agrees with the quantiles of Table 2 and reaches the same conclusion from the shape of the whole distribution rather than from one quantile.

3.5. Velocity Spread and Velocity Correlation Length

The networks combine two effects that the 1D experiment of Sect. 2.4 holds apart, and the third question posed in Sect. 1 asks how each of them acts. The homogeneous case of that experiment is the same run that verified the integrator in Sect. 3.1, where it recovers Eq. (14) to within 0.29 %, so it serves here as the baseline. Adding velocity spread lifts the CV above Eq. (14), and the correlation length decides by how much (Fig. 4c). At Pe = 501 the CV is 0.669 when a particle keeps its velocity across the whole domain, 0.355 at $\ell_c = 0.25$ L and 0.196 at $\ell_c = 0.05$ L.

In the perfectly correlated case the residence time is just L/U_i, so the CV approaches the analytical value $\sqrt{(e^{\sigma_v^2} - 1)} = 0.658$, which the simulation returns as 0.669 at Pe = 501. Two quantities therefore move in opposite directions as Pe rises. The CV falls toward this floor, while its excess over $\sqrt{(2/Pe)}$ grows, and the two should not be confused. A bundle of unmixed stream tubes is thus an upper bound on tailing rather than a representative pore network, and the finite correlation lengths are the cases that resemble the networks of Sect. 3.3.

3.6. Implications for Reactive Transport

Several problems that look separate all need exactly the distribution computed here. In reactive transport, any process whose extent depends on contact time, such as sorption with memory, slow dissolution or microbial uptake, is an average of the rate law over the whole age distribution rather than a function of the mean age. This is the exposure-time construction of Ginn (1999), and the moment and transform results of Sect. 2.1 supply the distribution it needs. The same distribution is the transit time distribution of catchment hydrology, where it governs the release of stored solutes and the chemistry of streamflow and where storage-selection functions give the modern formulation (Botter et al. 2011; Rinaldo et al. 2015; Harman 2015). In groundwater dating, the quantity read from environmental tracers is a moment, or a tracer-weighted average, of the same distribution (Cornaton and Perrochet 2006), and the joint distribution of age and life expectancy is the natural extension (Engdahl et al. 2013).

For that distribution the results above point to connectivity, not dimension, as the control, and that has a practical consequence. All of the processes just listed are dominated by the old-water end of the distribution, and it is precisely that end which a flat section misrepresents once the pore space is blocked. Where the pore space is well connected a flat section reproduces the full 3D distribution to within 5 % in CV and 2.5 % in the tail quantile, so it is a defensible economy. Where cementation, fines or precipitation have partly blocked it, the flat section places the old-water end nearly four times too high and leaves 5.4 times more pore volume without flow. A reactive-transport model built on such a section would overstate slow reaction extents in the same proportion, and close to the threshold it would do so unpredictably.

This suggests a cheap test that can be applied before any transport simulation is run. The fraction of open throats at which a network loses its connected paths depends only on the pore geometry, so it can be estimated from the image itself. Where a pore space sits comfortably above that fraction, a flat section will serve. Where it does not, the full 3D structure should be resolved.

Alongside that recommendation, five limitations frame the natural extensions of this work. First, the pore networks are regular grids with randomly assigned throat conductances rather than segmented images of real rock, so the number of throats per pore is idealized. The connectivity mechanism does not depend on the grid, but the numerical thresholds do. Second, pore bodies are treated as well mixed, which is the standard network assumption and applies the Eq. (12) limit at pore level, so incomplete mixing inside a pore is not represented. Third, the analytical limits of Sect. 2.2 assume steady flow and Fickian dispersion, and Sect. 3.4 shows where that assumption fails. Fourth, the solute treated here does not react, so letting reaction depend on age, such that older fluid is also more reacted, would close the loop with mixing-limited kinetics. Fifth, the age and life-expectancy fields reported here are means, whereas the full joint distribution of the two, reachable through the transform of Sect. 2.1, would resolve not only how old the fluid is but how much longer it will stay reactive.

4. Conclusion

Three questions were put in Sect. 1. Do the age-resolved equations return their own analytical limits, how much of the age distribution survives when the pore space is reduced to a plane, and what sets the width of that distribution. Labeling the fluid by its age makes the distribution computable. The zeroth age moment returns ordinary transport, the first and second moments obey transport equations for the mean age and the age variance, and a transform in the age variable carries the whole distribution in one function. Solved numerically, those moment equations return the analytical mean age exactly and the analytical age variance to within 0.11 % for Pe ≥ 20, which shows the two halves of the theory to be consistent. They also show that the familiar result $a = x/v$ picks up a correction of order 1/Pe as soon as the outlet is closed.

Applied to matched 2D and 3D pore networks, the same equations show that the number of resolved dimensions is immaterial while the pore space is fully connected and decisive once connections are removed. At 45 % of throats blocked, a flat section places the upper tail of the residence time distribution 3.8 times too high and the stagnant pore fraction 5.4 times too high. Near the threshold it yields a tail whose scatter between realizations exceeds its own mean. Spanning probabilities measured on the same grids put the flat loss of connection between 50 and 60 % of throats blocked while the cubic grid still spans at 70 %, which identifies lost connections as the cause. In the blocked networks the resolved tail is a power law with an exponent of −2.4 in 2D against −5.9 in 3D, the shallower exponent confirming the heavier flat tail, while at full connectivity the tail is too short to identify a form. Spreading the pore velocities lifts the CV above its value for uniform velocity, by an amount the velocity correlation length controls, with a bundle of unmixed stream tubes marking an upper bound rather than a typical case.

The practical consequence is a test that costs nothing to apply. Because the fraction of open throats at which a network loses its connected paths depends only on the pore geometry, it can be estimated from an image before any flow is computed. A pore space that sits comfortably above that fraction can be modeled on a plane, and its age distribution will be reproduced. A pore space that does not should be resolved in three dimensions, because the mean age survives the reduction but the old-water tail, which is what slow reactions respond to, does not.

Code and Data Availability

All computations were carried out in Python using NumPy and SciPy. The code and data are available from the corresponding author on request and will be delivered by email. No measured data were generated in this study.

Author Contributions

SA designed the study, carried out the derivations and computations, produced the figures, and wrote the manuscript.

Competing Interests

The author declares that he has no conflict of interest.

Use of Generative Artificial Intelligence

The author used a large language model to edit the manuscript for grammar and readability. The author reviewed and verified all content, results and figures, and takes full responsibility for the work.

References

Aris, R. (1956). On the dispersion of a solute in a fluid flowing through a tube. Proceedings of the Royal Society A 235, 67–77.

Bear, J. (1972). Dynamics of Fluids in Porous Media. American Elsevier, New York.

Berkowitz, B., Cortis, A., Dentz, M., Scher, H. (2006). Modeling non-Fickian transport in geological formations as a continuous time random walk. Reviews of Geophysics 44, RG2003.

Bijeljic, B., Mostaghimi, P., Blunt, M. J. (2011). Signature of non-Fickian solute transport in complex heterogeneous porous media. Physical Review Letters 107, 204502.

Bijeljic, B., Raeini, A., Mostaghimi, P., Blunt, M. J. (2013). Predictions of non-Fickian solute transport in different classes of porous media using direct simulation on pore-scale images. Physical Review E 87, 013011.

Blunt, M. J., Bijeljic, B., Dong, H., Gharbi, O., Iglauer, S., Mostaghimi, P., Paluszny, A., Pentland, C. (2013). Pore-scale imaging and modelling. Advances in Water Resources 51, 197–216.

Botter, G., Bertuzzo, E., Rinaldo, A. (2011). Catchment residence and travel time distributions: the master equation. Geophysical Research Letters 38, L11403.

Cornaton, F., Perrochet, P. (2006). Groundwater age, life expectancy and transit time distributions in advective-dispersive systems: 1. Generalized reservoir theory. Advances in Water Resources 29, 1267–1291.

Danckwerts, P. V. (1953). Continuous flow systems: distribution of residence times. Chemical Engineering Science 2, 1–13.

Deleersnijder, E., Campin, J.-M., Delhez, E. J. M. (2001). The concept of age in marine modelling: I. Theory and preliminary model results. Journal of Marine Systems 28, 229–267.

Delhez, E. J. M., Campin, J.-M., Hirst, A. C., Deleersnijder, E. (1999). Toward a general theory of the age in ocean modelling. Ocean Modelling 1, 17–27.

Dentz, M., Le Borgne, T., Englert, A., Bijeljic, B. (2011). Mixing, spreading and reaction in heterogeneous media: a brief review. Journal of Contaminant Hydrology 120–121, 1–17.

Engdahl, N. B., Ginn, T. R., Fogg, G. E. (2013). Using groundwater age distributions to estimate the effective parameters of Fickian and non-Fickian models of solute transport. Advances in Water Resources 54, 11–21.

Ginn, T. R. (1999). On the distribution of multicomponent mixtures over generalized exposure time in subsurface flow and reactive transport. Water Resources Research 35, 1395–1407.

Goode, D. J. (1996). Direct simulation of groundwater age. Water Resources Research 32, 289–296.

Harman, C. J. (2015). Time-variable transit time distributions and transport: theory and application to storage-dependent transport of chloride in a watershed. Water Resources Research 51, 1–30.

Kitanidis, P. K. (1994). The concept of the dilution index. Water Resources Research 30, 2011–2026.

Kreft, A., Zuber, A. (1978). On the physical meaning of the dispersion equation and its solutions for different initial and boundary conditions. Chemical Engineering Science 33, 1471–1480.

Le Borgne, T., Dentz, M., Carrera, J. (2008). Lagrangian statistical model for transport in highly heterogeneous velocity fields. Physical Review Letters 101, 090601.

Levenspiel, O. (1999). Chemical Reaction Engineering, 3rd ed. Wiley, New York.

Metzler, R., Klafter, J. (2000). The random walk's guide to anomalous diffusion: a fractional dynamics approach. Physics Reports 339, 1–77.

Renard, P., Allard, D. (2013). Connectivity metrics for subsurface flow and transport. Advances in Water Resources 51, 168–196.

Rinaldo, A., Benettin, P., Harman, C. J., Hrachowitz, M., McGuire, K. J., van der Velde, Y., Bertuzzo, E., Botter, G. (2015). Storage selection functions: a coherent framework for quantifying how catchments store and release water and solutes. Water Resources Research 51, 4840–4847.

Stauffer, D., Aharony, A. (1994). Introduction to Percolation Theory, 2nd ed. Taylor and Francis, London.

Taylor, G. I. (1953). Dispersion of soluble matter in solvent flowing slowly through a tube. Proceedings of the Royal Society A 219, 186–203.

van der Laan, E. T. (1958). Notes on the diffusion-type model for the longitudinal mixing in flow. Chemical Engineering Science 7, 187–191.

Varni, M., Carrera, J. (1998). Simulation of groundwater age distributions. Water Resources Research 34, 3271–3281.

Appendix A. Derivation of the Main-Text Equations

This appendix collects the derivation of the fifteen numbered relations, with full steps and in the notation of the main text. Throughout, $C(x, \tau, t)$ is the age-resolved concentration, the mass of solute per unit fluid volume with age between τ and $\tau + d\tau$, u is the pore velocity with $\nabla \cdot u = 0$, and D is the dispersion coefficient.

A.1 Age-Resolved Concentration and Its Moments, Equations (1) and (2)

Equation (1) defines the ordinary concentration as the zeroth age moment, the total over all ages. Equation (2) defines the age concentration as the first moment and the mean age as their ratio, $a = \alpha/c$. Both are definitions and require no derivation.

A.2 The Aging Equation and Consistency with Transport, Equations (3) and (4)

Age advances at exactly the rate of time, which appears as transport along the age axis at unit speed and contributes the term $\partial C/\partial \tau$. The age-resolved concentration therefore satisfies Eq. (3). Integrating Eq. (3) over all ages requires $\int_0^\infty \partial C/\partial \tau \, d\tau = [C]_0^\infty = C(\infty) - C(0)$. The first term vanishes because no parcel is infinitely old. The second vanishes in the interior because there is no interior source of zero-age water, all zero-age fluid entering through the inflow boundary; this is the condition stated in the main text. The aging term therefore drops and Eq. (4) follows.

A.3 Mean Age and Life Expectancy, Equations (5) and (6)

Multiplying Eq. (3) by τ and integrating over age, the aging term integrates by parts to $\int_0^\infty \tau \, (\partial C/\partial \tau) \, d\tau = [\tau C]_0^\infty - \int_0^\infty C \, d\tau = -c$, since τC vanishes at both limits. The remaining terms give Eq. (5), a transport equation for α with a uniform unit source c. The mirror image of age is the life expectancy, obtained by running the same problem backward, with the flow reversed and the inlet and outlet exchanged, giving Eq. (6) with the same unit source.

A.4 The Moment Recursion and the Age Variance, Equations (7) and (8)

Defining $\mu_n = \int_0^\infty \tau^n C \, d\tau$, multiplying Eq. (3) by τ^n and integrating at steady state, the aging term again integrates by parts, $\int_0^\infty \tau^n \, (\partial C/\partial \tau) \, d\tau = -n \, \mu_{n-1}$, giving the recursion Eq. (7). The zeroth moment is c and the first is α; the second is forced by 2α and yields the age variance Eq. (8) as $\sigma_a^2 = \langle \tau^2 \rangle - \langle \tau \rangle^2 = \mu_2/c - a^2$.

A.5 Laplace Transform and Moment Generation, Equations (9) and (10)

The age coordinate is handled by a Laplace transform $\hat{C}(x, s) = \int_0^\infty C \, e^{-s\tau} \, d\tau$. The aging term transforms as $\int_0^\infty (\partial C/\partial \tau) \, e^{-s\tau} \, d\tau = s \, \hat{C} - C(0) = s \, \hat{C}$, so the transform variable enters as a uniform first-order decay, giving Eq. (9). Evaluated in the outflow, $\hat{C}$ is the transfer function of the residence time distribution and the standard moment-generating property gives Eq. (10).

A.6 Analytical Residence Time Distributions, Equations (11) to (14)

With advection only ($D = 0$) along a path of length L at speed v, every parcel has the same history and the distribution is a single spike, Eq. (11). In a perfectly mixed reservoir the outflow is a fair sample of the interior and the distribution is exponential with T the ratio of fluid volume to volumetric flow rate, Eq. (12). Between these limits, 1D advection–dispersion gives the first-passage density of a drifting diffusion, the inverse-Gaussian, Eq. (13). Its mean is L/v and its variance $2 D L / v^3$, so the squared coefficient of variation is $(2 D L / v^3)(v/L)^2 = 2 D/(v L) = 2/Pe$, Eq. (14).

A.7 The Closed-Outlet Correction, Equation (15)

For 1D steady flow Eq. (5) reduces to $v a' - D a'' = 1$ with $a(0) = 0$. The general solution is $a = x/v + A + B e^{vx/D}$. Under a semi-infinite or advective-outflow condition boundedness forces $B = 0$ and then $A = 0$, giving $a = x/v$ exactly and independently of D. Under a zero-gradient outlet condition $a'(L) = 0$ instead, which gives $B = -(D/v^2) e^{-Pe}$ and $A = (D/v^2) e^{-Pe}$, so that $a(L) = L/v - (D/v^2)(1 - e^{-Pe})$, Eq. (15). The relative deficit is $(1/Pe)(1 - e^{-Pe})$, which is 19.9 % at Pe = 5 and 1.0 % at Pe = 100, in agreement with Table 1.

Appendix B. Reference Implementations

The listings below are extracted verbatim from the deposited scripts and reproduce the numbered equations. Comments cross-reference the equations, so that the inverse-Gaussian density is Eq. (13), the analytical form $CV^2 = 2/Pe$ is Eq. (14), and the closed-outlet correction is Eq. (15).

B.1 Inverse-Gaussian Residence Time Distribution and Its CV

```
import numpy as np

# Inverse-Gaussian residence time distribution and CV for 1-D advection–dispersion.
# Time tau is in units of the advective mean L/v, so the mean is 1 and the shape is Pe/2.
def rtd_inverse_gaussian(tau, Pe):
    lam = Pe / 2.0                                  # shape parameter = Pe/2
    return np.sqrt(lam/(2*np.pi*tau**3)) * np.exp(-lam*(tau-1.0)**2/(2.0*tau))   # Eq (13)

def cv_residence_time(Pe):
    return np.sqrt(2.0 / Pe)                        # CV^2 = 2/Pe   (Eq 14)
```

B.2 Consistency with the Published Dispersion-Model Variances

```
import numpy as np

# Consistency check (Figure 3a): CV^2 = 2/Pe (Eq 14) is the leading term of the exact
# axial-dispersion-model variances of classical reactor theory. Agreement at large Pe is
# therefore analytic, not independent evidence; the boundary condition sets the correction.
Pe = np.logspace(0, 3, 400)
cv2_theory = 2.0/Pe                                 # Eq (14)
cv2_open   = 2.0/Pe + 8.0/Pe**2                     # open vessel  (van der Laan 1958)
cv2_closed = 2.0/Pe - (2.0/Pe**2)*(1.0-np.exp(-Pe))  # closed vessel (Danckwerts 1953)
# At Pe = 100 the open- and closed-vessel variances differ from 2/Pe by 4% and 1%.
```

B.3 Random-Walk Particle Tracking

This listing is the deposited routine in full, including the exit horizon and the reporting of the unexited fraction, which the earlier version of this appendix omitted.

```
import numpy as np, math

# First-passage (residence) time of an ensemble to the outlet x = L, independent of the
# analytical derivation. Each step: x += U*dt + sqrt(2*D*dt)*xi, with Pe = U*L/D.
```

```
# Each particle redraws its velocity every correlation length lc; lc = inf is the
# perfectly correlated (stratified) limit. The censored fraction is returned, not discarded.
def first_passage(Pe, N=8000, L=1.0, U=1.0, sv=0.6, lc=np.inf, dt=None, seed=7, tmax=40.0):
    rng = np.random.default_rng(seed)
    D = U*L/Pe
    if dt is None:                      # scale the step with D so the diffusive
        dt = min(0.0008*L/U, 0.02*L*L/max(D,1e-12)*0.02)   # increment is a fixed
        dt = max(dt, 1e-5)                                  # small fraction of L
    sq = math.sqrt(2*D*dt)
    x = np.zeros(N); out = np.full(N, np.nan); act = np.ones(N, bool); t = 0.0
    drw = lambda m: U*np.exp(sv*rng.standard_normal(m) - 0.5*sv**2)
    Ui = drw(N); nxt = np.full(N, lc if np.isfinite(lc) else np.inf)
    while act.any() and t < tmax:       # exit horizon; censored fraction reported
        m = int(act.sum())
        x[act] += Ui[act]*dt + sq*rng.standard_normal(m)
        t += dt
        if np.isfinite(lc):
            nd = act & (x >= nxt)
            if nd.any(): Ui[nd] = drw(int(nd.sum())); nxt[nd] += lc
        d = act & (x >= L); out[d] = t; act[d] = False
    return out[~np.isnan(out)], float(np.isnan(out).mean())   # times, censored fraction
```

B.4 Pore Network, Pressure, the Age Equations and Particle Tracking

The network solver assembles the pressure system only on the pores that actually connect the inlet face to the outlet face. The fixed-pressure pores are eliminated, which leaves a symmetric positive definite matrix, so conjugate gradients converges in 3D, where a direct factorization is impractical. Because potential flow is downhill in pressure the flow graph is acyclic, so Eqs. (5) and (7) are solved exactly by a single sweep through the pores in order of decreasing pressure.

```
# Network form of Eq. (5) and Eq. (7). Qout_i is the total outflow of pore i,
# including flow leaving through the outlet face; V_i is the pore volume.
#
#   Eq (5):  Qout_i a_i  - sum_(j upstream) q_ji a_j  = V_i
#   Eq (7):  Qout_i m2_i - sum_(j upstream) q_ji m2_j = 2 V_i a_i
#
order = np.argsort(-p, kind="stable")        # most upstream first (highest pressure)
for k in range(n):
    i = order[k]
    s, e = bnd[k], bnd[k+1]                  # incoming throats of pore i
    if e > s:
        w = q_s[s:e]; u = up_s[s:e]
        a[i]  = (Vs[i] + float(w @ a[u])) / Q[i]
        m2[i] = (2.0*Vs[i]*a[i] + float(w @ m2[u])) / Q[i]
    else:
        a[i]  = Vs[i] / Q[i]
        m2[i] = 2.0*Vs[i]*a[i] / Q[i]
var = np.maximum(m2 - a**2, 0.0)             # Eq (8)
```